

一种水稳性的Zn基金属-有机框架的合成及其对铁离子及2,6-二氯-4-硝基苯胺的荧光识别

王晓晴* 马学慧 冯豆豆 唐婧 吴丹

(中北大学理学院化学系, 太原 030051)

摘要: 以3,5-双(4-羧基苯氧基)吡啶(H_2bcpp)和1,4-双(1-咪唑基)苯(1,4-bib)为配体,通过溶剂热法构筑了一个新型的热稳定性和水稳定性的Zn(II)基金属-有机框架: $[Zn_2(bcpc)_2(1,4-bib)_2] \cdot 1.5H_2O$ (**1**)。配合物**1**属于单斜晶系, $I2/a$ 空间群,具有一维管状结构。相邻的一维结构通过相互穿插形成一个三维超分子结构。此外,配合物**1**具有良好的荧光性,能够对水溶液中的铁离子及农药2,6-二氯-4-硝基苯胺实现高灵敏及高选择的荧光猝灭检测。

关键词: 金属-有机框架; Zn(II); 荧光检测; 铁离子; 农药

中图分类号: O614.24[†] 文献标识码: A 文章编号: 1001-4861(2022)01-0137-08

DOI: 10.11862/CJIC.2022.015

Synthesis of a Water-Stable Zn(II)-Based Metal-Organic Framework for Luminescence Detecting Fe^{3+} and 2,6-Dichloro-4-nitroaniline

WANG Xiao-Qing* MA Xue-Hui FENG Dou-Dou TANG Jing WU Dan

(Department of Chemistry, College of Science, North University of China, Taiyuan 030051, China)

Abstract: A novel thermal-stable and water-stable Zn(II)-based metal-organic framework (MOF), $[Zn_2(bcpc)_2(1,4-bib)_2] \cdot 1.5H_2O$ (**1**) was synthesized by solvothermal method based on 3,5-bis(4-carboxylphenoxy)pyridine (H_2bcpp) and 1,4-bis(1-imidazolyl)benzene (1,4-bib). Complex **1** belongs to the monoclinic system with space group $I2/a$, which exhibits a 1D tubular structure. The adjacent 1D tubular structures are interpenetrated with each other to obtain a 3D supramolecular structure. Moreover, complex **1** exhibits excellent photoluminescence property, which can be applied as a “turn-off” fluorescence probe to detect Fe^{3+} ion and pesticide 2,6-dichloro-4-nitroaniline in an aqueous solution with high selectivity and sensitivity. CCDC: 2095435.

Keywords: metal-organic framework; Zn(II); luminescence detecting; Fe^{3+} ; pesticide

0 Introduction

Currently, the large discharge of hazardous pollutants from agriculture, mines, and factories has brought serious damage to the ecological environment and physical health. For example, organochlorine pesticides have been widely applied to kill off insect pests and improve the yield of crops^[1]. The 2,6-dichloro-4-

nitroaniline (DCN) is one of organochlorine pesticides, which is a broad-spectrum insect killer and can be used to prevent cotton rotten bells, wheat powdery mildew, and garden stuff rot^[2]. Whereas the degradation of DCN needs a long time, and the ingestion of DCN residues on food can damage the immune system of humans and cause cancer or other illnesses. Moreover,

收稿日期: 2021-05-24。收修改稿日期: 2021-10-21。

国家自然科学基金(No. 21601163, 22078309)、山西省高等学校科技创新项目(No. 2019L0579)和中北大学青年学术带头人(No. QX201906)资助。

*通信联系人。E-mail: xqwang@nuc.edu.cn

Fe^{3+} ions exist in living systems that take part in some cellular processes, such as oxygen transport and hemoglobin formation^[3]. However, the excess of Fe^{3+} ions can lead to some diseases of proteins and nucleic acids. Thus, exploring a rapid and effective detecting method to sense metal ions and organochlorine pesticides is significant.

The fluorescence sensor exhibits rapid response, high sensitivity, selectivity, and simple operation for detecting pollutants. Recently, metal-organic frameworks (MOFs) as novel fluorescence sensors have been used to detect pollutants, including heavy metal cations (Fe^{3+} , Hg^{2+} , Cu^{2+}), inorganic anions (F^- , $\text{Cr}_2\text{O}_4^{2-}$, MnO_4^{2-}), pesticides (organochlorine pesticides, organophosphorus pesticides), nitrobenzene, and so on^[4-8], which can be attributed to their high surface areas, diverse chemical and physical properties, excellent fluorescence properties and abundant action sites. Among them, these MOFs based on d^{10} metal centers (Zn^{2+} , Cd^{2+}) and the conjugated ligands have been potentially used as photoluminescent probe materials to detect pollutants due to their excellent fluorescence properties. Nevertheless, the stability of MOFs is still a significant challenge for practical applications as fluorescence sensors in an aqueous solution.

The hard-soft-acid-base (HSAB) theory indicates that the $\text{Zn}(\text{II})$ is a relatively soft-acid ion, which has stronger coordination bonding with the soft-base N-donor ligands^[9]. But the strong coordination bonds could lead to poor crystallinity. Based on the guidelines, we chose mixed ligands (rigid N-donor ligand and flexible carboxylic ligand) to construct a 1D rhombic nanotube structure with high stability and crystallinity, $[\text{Zn}_2(\text{bcpp})_2(1,4\text{-bib})_2] \cdot 1.5\text{H}_2\text{O}$ (**1**) (H_2bcpp =3,5-bis(4-carboxylphenoxy)pyridine, 1,4-bib=1,4-bis(1-imidazolyl)benzene). Based on the high water stability and excellent luminescent property, complex **1** was used as a multi-responsive sensor to detect metal ions and pesticides in aqueous solutions and real samples.

1 Experimental

1.1 Materials and methods

All reagents and materials were commercially

available and used directly without further purification. The ligands H_2bcpp and 1,4-bib were obtained from Jinan Henhua Sci. & Technol. Co., Ltd. Powder X-ray diffraction (PXRD) patterns were performed with a Rigaku Dmax 2500 diffractometer (XRD, $\text{Cu K}\alpha$, $\lambda = 0.154$ nm, $U=40$ kV, $I=25$ mA, $2\theta=5^\circ-50^\circ$). Infrared spectra were obtained at FTIR-8400S spectrometer and thermogravimetric analysis (TGA) curves were carried out with a ZCT-A analyzer. UV-Vis absorption experiments were performed with a Shimadzu UV-2600 spectrophotometer. Photo-luminescence spectra were taken on a Hitachi F-4600 fluorescence spectrophotometer.

1.2 Synthesis of $[\text{Zn}_2(\text{bcpp})_2(1,4\text{-bib})_2] \cdot 1.5\text{H}_2\text{O}$ (**1**)

A mixture of $\text{Zn}(\text{NO}_3)_2 \cdot 6\text{H}_2\text{O}$ (0.016 mmol, 4.8 mg), H_2bcpp (0.008 0 mmol, 2.8 mg), 1,4-bib (0.016 mmol, 3.4 mg) in $\text{EtOH}/\text{H}_2\text{O}$ (4.0 mL, 1:3, V/V) was sealed in a 25 mL reactor, heated to 120 °C for 55 h, and then cooled to room temperature. Colorless block crystals were obtained by washed with EtOH , filtration and dried in air. Anal. Calad. for $\text{C}_{68}\text{H}_{52}\text{N}_8\text{O}_8\text{Zn}_2$ (%): C, 65.81; H, 4.19; N, 9.03. Found(%): C, 65.77; H, 4.22; N, 9.06. IR(KBr, cm^{-1}): 3 789(w), 3 122(w), 2 358(s), 1 674(m), 1 677(w), 1 569(m), 1 554(m), 1 539(m), 1 521(w), 1 488(m), 1 452(m), 1 429(m), 1 406(m), 1 379(m), 1 307(m), 1 294(m), 1 263(m), 1 026(m), 999 (m), 954(w), 838(m), 729(m), 653(m) (Fig.S1, Supporting information).

1.3 Crystal structure determination

The crystal data of **1** were collected on a Rigaku Oxford Diffraction XtaLAB Synergy - S diffractometer with $\text{Cu K}\alpha$ radiation ($\lambda=0.154$ 184 nm) at 150 K. Its structure was solved by the superfilp method in Olex2 program. All non-hydrogen atoms were refined on F^2 with full-matrix least-squares procedures in SHELXL-2016. Some free disordered solvent molecules were removed with the PLATON/SQUEEZE routine. The SQUEEZE result reveals a residual electron density of 141 electrons/cell ($Z=8$) which corresponds to the residual electron density of 1.5 H_2O molecules. The free 1.5 H_2O molecules were also proved by the TGA and elemental analysis. The crystal data and refined parameters are presented in Table 1. Some selected bond distanced and angles are listed in Table S1.

Table 1 Crystal data and refined parameters of complex **1**

Parameter	1
Formula	$C_{68}H_{52}N_8O_8Zn_2$
Formula weight	1 239.91
Crystal system	Monoclinic
Space group	$I2/a$
a / nm	1.683 61(3)
b / nm	2.566 63(4)
c / nm	2.778 46(5)
$\beta / (^\circ)$	98.905(2)
Z	8
V / nm^3	11.861 6(4)
$D_c / (\text{g} \cdot \text{cm}^{-3})$	1.389
μ / mm^{-1}	1.520
$F(000)$	5 120.0
Unique reflection	39 446
Observed reflection [$I > 2\sigma(I)$]	11 716
Parameter	1 162
GOF	1.070
Final R indices [$I > 2\sigma(I)$]	$R_1=0.072\ 1, wR_2=0.205\ 0$
R indices (all data)	$R_1=0.085\ 2, wR_2=0.215\ 9$

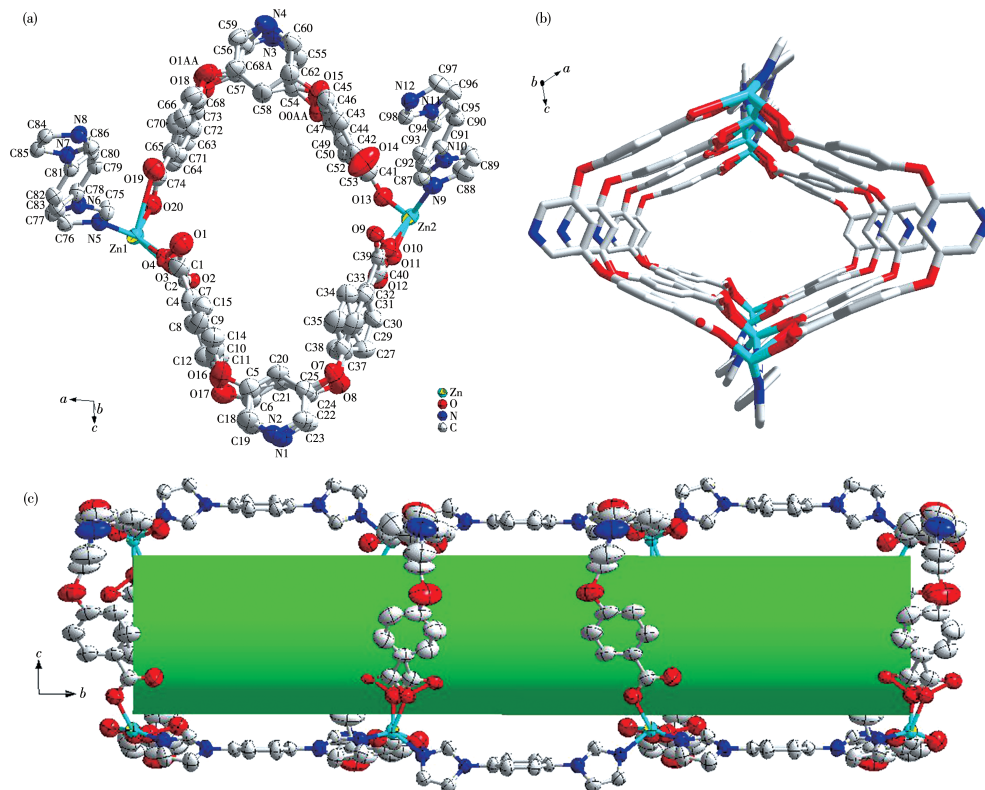
CCDC: 2095435.

2 Results and discussion

2.1 Crystal structure of complex **1**

Single-crystal X-ray diffraction analysis presents that complex **1** crystallizes in the monoclinic with space group $I2/a$. Fig. 1a displays that the asymmetric unit contains two Zn(II) ions, two bcpp^{2-} ligands, two 1,4-bib ligands, where the free disordered solvent molecules are omitted. The dihedral angles between two benzene rings in two different bcpp^{2-} ligands are $40.941(331)^\circ$ and $50.180(265)^\circ$, respectively (Fig. S2). Both Zn(II) ions are four-coordinated by two nitrogen atoms from different 1,4-bib ligands and two oxygen atoms from two bcpp^{2-} ligands with a distorted tetrahedral geometry. The average bond distances of Zn—N and Zn—O are in the ranges of 0.200 2–0.202 7 nm and 0.187 7–0.202 8 nm, respectively, which are in accordance with the reported values previously^[10].

In complex **1**, H_2bcpp ligands are completely



All of the hydrogen atoms are omitted for clarity

Fig. 1 Asymmetric unit of **1** with 50% thermal ellipsoid probability (a); 1D tubular structure of complex **1** along b axis (b) and along a axis (c) with 50% thermal ellipsoid probability

deprotonated. Each carboxylate group of bcpp^{2-} bridges one $\text{Zn}(\text{II})$ ion, which exhibits the coordination mode of η^1 . Two bcpp^{2-} ligands bridge two $\text{Zn}(\text{II})$ ions to form a ring. The adjacent rings are linked by two 1,4-bib ligands, to form a 1D tubular structure with a rhombic channel (the diagonal length of 1.5 nm \times 1.9 nm, Fig. 1b and 1c). Because of the large rhombic windows in **1**, the adjacent 1D tubular structures are interpenetrated with each other. Moreover, the imidazole rings of the adjacent 1,4-bib ligands exist two $\pi\cdots\pi$ stacking interactions with face-to-face fashion, but two imidazole

rings are not exactly parallel (Fig. 2a). One is the π -stacking interaction between Cg1 plane and Cg3 plane (Cg1: N5-C75-N6-C77-C76, Cg3: N9-C87-N10-C89-C88, centroid \cdots centroid 0.376 93 nm, dihedral angle 4.7 $^\circ$). The other is the π -stacking interaction between Cg2 plane and Cg4 plane (Cg2: N7-C85-C84-N8-C86, Cg4: N11-C96-C97-N12-C98, centroid \cdots centroid 0.378 77 nm, dihedral angle 1.4 $^\circ$). The adjacent 1D tubular structures are interpenetrated and linked by weak π -stacking interactions to form a 3D supramolecular structure (Fig. 2b).

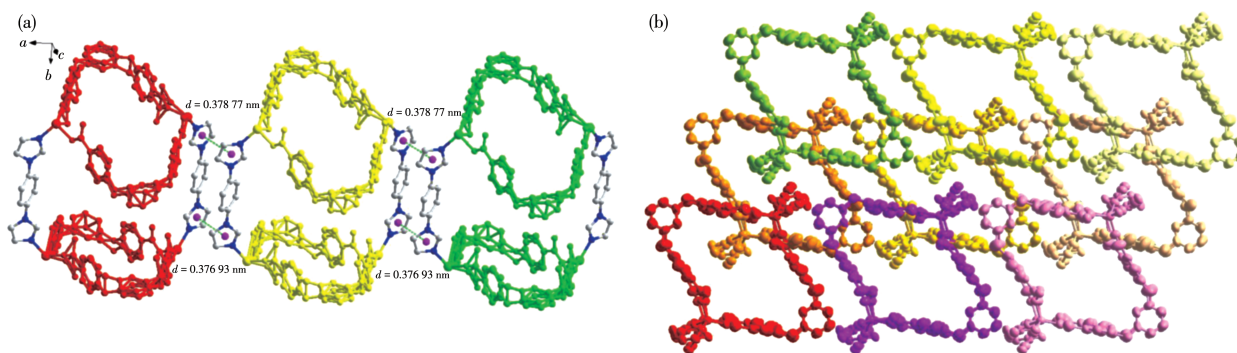


Fig.2 (a) π -stacking interaction in complex **1**; (b) 3D supramolecular structure of **1** viewed along b axis with 50% thermal ellipsoid probability

2.2 PXRD and TGA

The thermal stability of **1** was studied under an N_2 atmosphere from 50 to 700 $^\circ\text{C}$ (Fig. S3). Complex **1** displayed a weight loss of 2.2% between 50 and 113 $^\circ\text{C}$ because of the loss of one and a half free H_2O molecules (Calcd. 2.1%). There was a platform from 113 to 326 $^\circ\text{C}$. Subsequently, there was a rapid weight loss

beyond 326 $^\circ\text{C}$ that indicates the decomposition of **1**. Furthermore, the PXRD pattern of **1** can match the simulated one, indicating its phase purity. The PXRD pattern of **1** after being soaked in boiling water almost had no change compared with the simulated one, indicating its water stability (Fig. 3).

2.3 Photoluminescence properties

The solid-state luminescence emission spectra of H_2bcpp ($\lambda_{\text{ex}}=355$ nm), 1,4-bib ($\lambda_{\text{ex}}=353$ nm), and **1** ($\lambda_{\text{ex}}=355$ nm) were investigated at room temperature (Fig. 4). H_2bcpp and 1,4-bib showed the main emission peaks at 463.8 and 475.2 nm, respectively. Their emission peaks may be ascribed to $\pi^* \rightarrow \pi$ or $\pi^* \rightarrow n^{[11-12]}$ transitions. Complex **1** exhibited a single intense broad emission band at 461.4 nm, which was close to the emission peak of H_2bcpp . Compared with the emission peaks of H_2bcpp and 1,4-bib, complex **1** presented a 2.4 nm blue shift and 13.8 nm blue shift in the luminescence emission spectrum, respectively. Considering that Zn^{2+} ions have a d^{10} configuration, the luminescence emission spectrum of **1** can be assigned to the

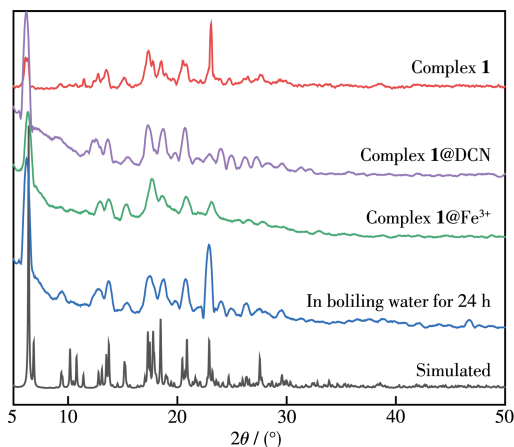


Fig.3 PXRD patterns of complex **1**, **1** after soaking in boiling water for 24 h, and **1** after detecting various analytes

metal-to-ligand charge transfer (MLCT) or ligand-to-metal charge transfer (LMCT)^[13-18]. The slightly blue-shifted emission bands can be attributed to the coordination effects. Based on the good luminescence property of complex **1**, we further studied the luminescence sensing activity of complex **1**.

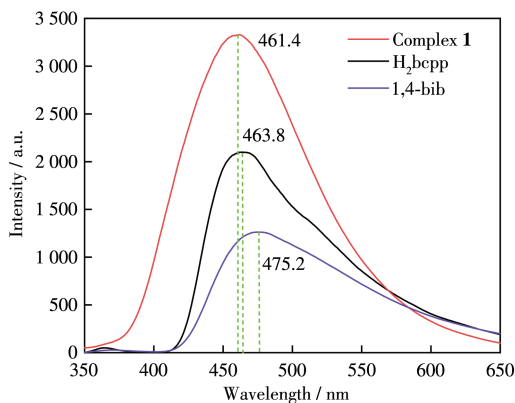


Fig.4 Solid-state luminescence emission spectra of H_2bcpp , 1,4-bis, and complex **1** at 298 K

2.4 Selective detection of Fe^{3+} ions

The detection ability of complex **1** for Fe^{3+} ions has been explored in an aqueous solution. The powder sample of **1** (2.0 mg) was evenly dispersed into 2.0 mL of $10 \text{ mmol} \cdot \text{L}^{-1} \text{ M}(\text{NO}_3)_n$ aqueous solution ($M^{n+} = \text{Na}^+, \text{Zn}^{2+}, \text{Ni}^{2+}, \text{Mg}^{2+}, \text{Mn}^{2+}, \text{Ca}^{2+}, \text{Ba}^{2+}, \text{Cu}^{2+}, \text{Cd}^{2+}, \text{Pb}^{2+}, \text{Co}^{2+}, \text{Cr}^{3+}, \text{Fe}^{2+}, \text{Al}^{3+}, \text{Fe}^{3+}$). The fluorescence emission spectra of the dispersed suspensions were measured at $\lambda_{\text{ex}} = 355 \text{ nm}$. As shown in Fig.5a, the luminescence intensity of **1** has an almost completely quenching with the addition of Fe^{3+} , indicating the excellent sensing ability for Fe^{3+} . The titration experiment was further performed to explore the sensing ability for Fe^{3+} ions (Fig. 5b). With adding the Fe^{3+} solution, the fluorescence intensity of **1** dropped gradually with a high fluorescent quenching efficiency of 93.3% in the presence of $1.3 \text{ mmol} \cdot \text{L}^{-1} \text{ Fe}^{3+}$ solution. Moreover, the low Fe^{3+} concentration and the fluorescence intensity exhibited a good

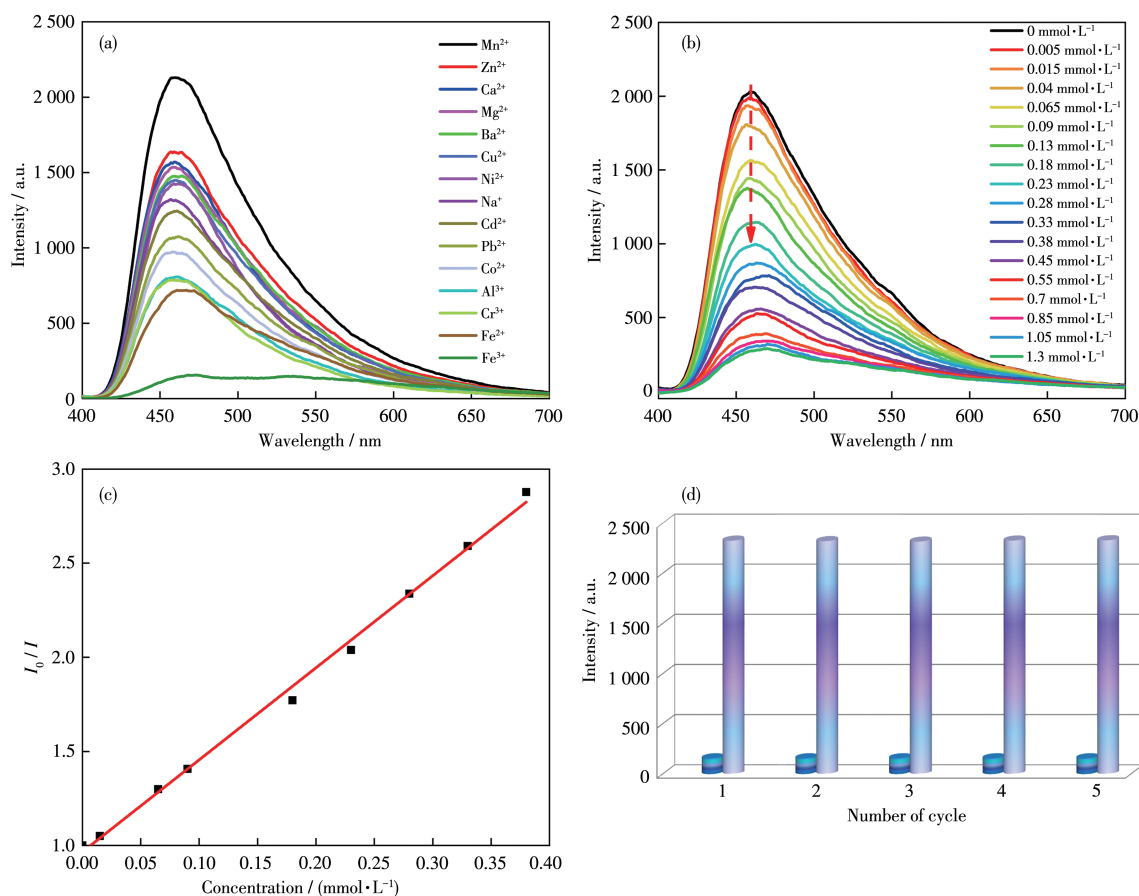


Fig.5 (a) Fluorescence intensity of **1** in aqueous solutions containing various metal cations at 461.4 nm ($\lambda_{\text{ex}} = 355 \text{ nm}$); (b) Titration experiment of **1** for detecting Fe^{3+} ; (c) Stern-Volmer plot of **1** for sensing Fe^{3+} in aqueous solution; (d) Repeatability experiment of **1** for detecting Fe^{3+}

linear relationship (Fig. 5c), which can be fitted to a line by Stern-Volmer relationship: $I_0/I = c_{\text{Fe}^{3+}} K_{\text{sv}} + 1$, where I_0 and I are the luminescence intensities of **1** without and with the addition of Fe^{3+} , respectively; K_{sv} is the Stern-Volmer constant. The K_{sv} was calculated to be $4.90 \times 10^3 \text{ L} \cdot \text{mol}^{-1}$. The limit of detection (LOD) was about $1.8 \mu\text{mol} \cdot \text{L}^{-1}$ calculated by $3\sigma/K_{\text{sv}}^{[19]}$. Compared with some reported MOFs-based fluorescence sensors, complex **1** exhibited a comparable or lower LOD for sensing Fe^{3+} in an aqueous solution (Table S2).

Furthermore, selectivity and recyclability are also important for evaluating the detecting ability of **1**. Thus, the anti-interference fluorescence detection experiments for Fe^{3+} ions were explored by adding Fe^{3+} ions into the suspension of complex **1** with various metal cations. It was found that the Fe^{3+} for the fluorescence intensity of complex **1** still had an outstanding quenching effect (Fig. S4). The result indicates that complex **1** exhibits good selectivity for Fe^{3+} . In addition, the recyclability of **1** for the detection of Fe^{3+} was verified by the cyclic tests. After repeated for five cycles, the fluorescence sensitivity remained almost unchanged (Fig. S5d). The results suggest that complex **1** has high sensitivity, selectivity, and recyclability for sensing Fe^{3+} . In addition, we conducted a time-dependent experiment and found that the fluorescence intensity decreased rapidly in 30 s and remained unchanged in 360 s (Fig. S5a). Herein, the recognition mechanism of **1** for sensing Fe^{3+} has been investigated. The PXRD peaks of complex **1** before and after recognizing Fe^{3+} ions almost had no change, indicating the structure of complex **1** keeps perfectly (Fig. 3). Compared with the UV-Vis spectra of other metal ions, the UV-Vis absorption spectra of Fe^{3+} had the greatest extent overlaps with the excitation spectra of complex **1** (Fig. S6a), which suggests that there is an inner filter effect (IFE) between complex **1** and Fe^{3+} . The excitation energy of complex **1** is absorbed by Fe^{3+} , which leads to fluorescence quenching^[20-21]. IR spectra, where **1**@ Fe^{3+} showed new peaks at $1\ 745$ and $1\ 411 \text{ cm}^{-1}$ compared with complex **1** (Fig. S1), further indicate that there is a weak interaction between complex **1** and Fe^{3+} .

2.5 Selective detection of DCN

Organochlorine pesticides as a class of widely-used pesticides have gained numerous attention from

environmentalists because residual organochlorine pesticides are harmful to the environment and human health. Thus, we try to investigate the detection ability of **1** ($\lambda_{\text{ex}} = 355 \text{ nm}$) for organochlorine pesticides in an aqueous solution. Herein, we selected eight pesticides to explore, including carbaryl, chlorobenzene (CB), atrazine, 2,4-dichlorobenzene (2,4-DCP), 1,2-dichlorobenzene (1,2-DiCB), 1,2,4-trichlorobenzene (1,2,4-TriCB), 1,2,4,5-tetrachlorobenzene (1,2,4,5-TetraCB), and DCN. As shown in Fig. 6a, DCN shows the highest quenching efficiency for the fluorescence intensity of **1** (81.8%). The titration experiments exhibited that the fluorescence intensity of **1** gradually reduced with adding DCN solution (Fig. 6b). In addition, the DCN concentration and the fluorescence intensity of complex **1** exhibited a good linear relationship (Fig. 6c). The K_{sv} for DCN was $2.06 \times 10^4 \text{ L} \cdot \text{mol}^{-1}$, and the LOD was about $0.44 \mu\text{mol} \cdot \text{L}^{-1}$, indicating the excellent sensitivity of **1** for DCN. Moreover, the selective and the anti-interference ability were investigated, which are shown in Fig. 6d and Fig. S7. The time-dependence experiment of complex **1** for DCN further proves that complex **1** has high stability (Fig. S5b). The results displayed high selectivity and recyclability, indicating that complex **1** is a potential fluorescent sensor for detecting DCN. Furthermore, **1** has higher sensitivity and lower LOD compared with some reported MOF fluorescent probes for detecting DCN (Table S3).

Additionally, the sensing ability of **1** for DCN in real samples, such as the concentrated juices of grapes, nectarines, and carrots, was also investigated (Fig. S8). Their K_{sv} and LOD values are listed in Table S4. Notably, the LOD values were all lower than the maximum DCN residue reported in China National Food Safety Standards^[22]. The results indicate the excellent selectivity, sensitivity, and recyclability of **1** for detecting DCN in aqueous solution and real samples. At the same time, complex **1** had a high recovery rate in these real samples (Table 2). Furthermore, the sensing mechanism of **1** was investigated. As shown in Fig. S6b, the excitation spectrum of complex **1** has a major overlap with the UV spectrum, indicating that there is an IFE^[25-26] between DCN and complex **1**. DCN absorbs the excitation energy of complex **1**, resulting in fluorescence quenching.

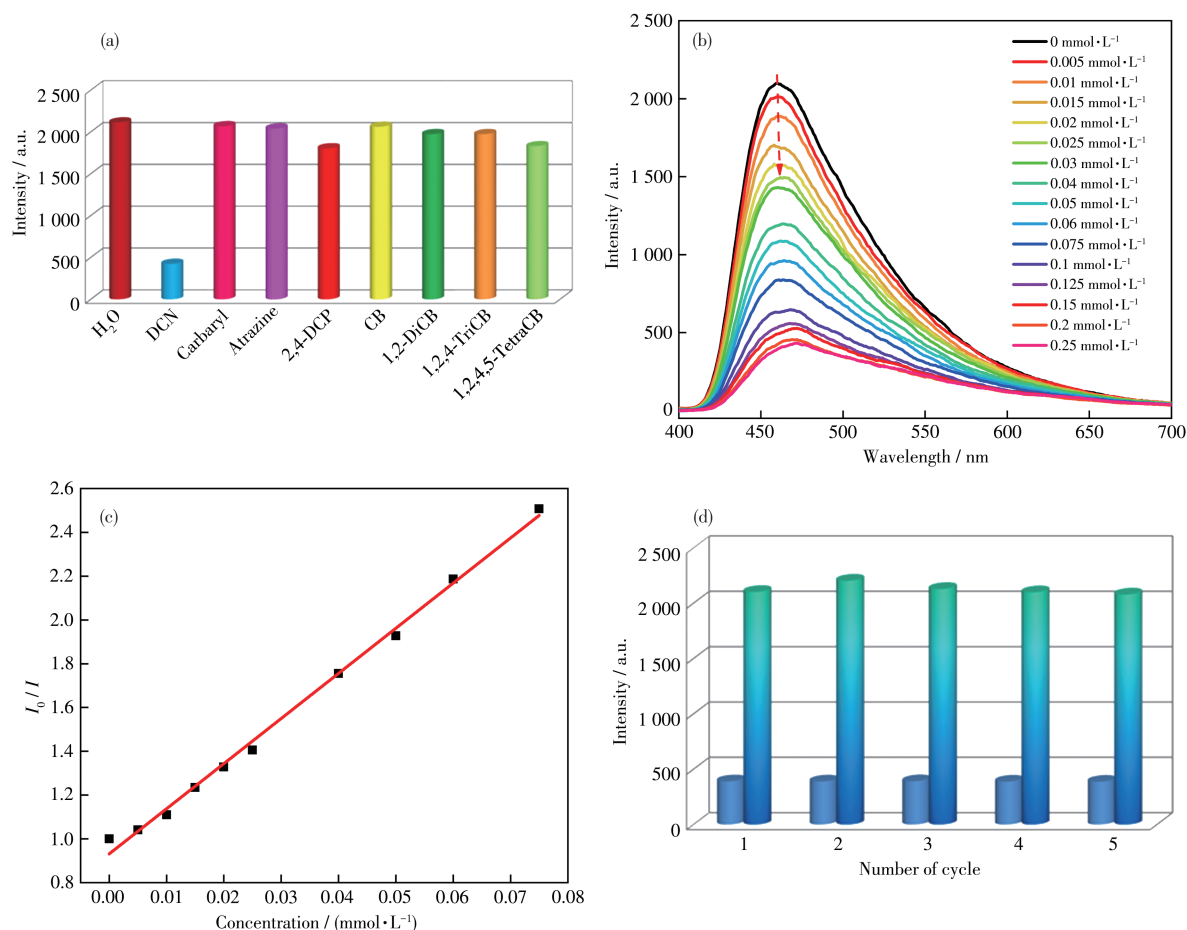


Fig.6 (a) Fluorescence intensity of **1** in various organochlorine pesticides at 461.4 nm ($\lambda_{ex}=355$ nm); (b) Titration experiment of **1** for DCN; (c) Stern-Volmer plot of **1** for sensing DCN; (d) Repeatability experiment of **1** for DCN

Table 2 Determination of DCN in real samples

Sample	Added / ($\mu\text{mol}\cdot\text{L}^{-1}$)	Recovery / %	Average recovery / %	RSD* / %
Carrot	10	94.1	94.7	0.17
	20	95.1		0.48
	30	94.8		1.28
Grape	10	103.0	99.7	0.85
	20	100.8		2.43
	30	95.2		1.46
Nectarine	10	110.1	99.2	1.22
	20	92.9		1.35
	30	94.6		2.01

* Relative standard deviation, $n=3$.

3 Conclusions

In summary, a novel water-stable Zn(II)-based MOF (**1**) was constructed with a flexible carboxylic ligand 3,5-bis(4-carboxylphenoxy)pyridine and a rigid N-donor ligand 1,4-bis(1-imidazoly)benzene. Complex **1** exhibits a 1D tubular structure, where the adjacent

1D tubular structures are interpenetrated with each other to obtain a 3D supramolecular structure. Furthermore, the photoluminescence property of **1** was investigated, which indicates that **1** can be used to detect Fe³⁺ ion and pesticide DCN in an aqueous solution. The LOD values for Fe³⁺ ion and DCN in aqueous solutions

are 1.8 and 0.44 $\mu\text{mol}\cdot\text{L}^{-1}$, respectively. The results suggested that complex **1** can be used as a “turn-off” fluorescence probe to trace Fe^{3+} ion and pesticide DCN with high selectivity, sensitivity, and recyclability.

Supporting information is available at <http://www.wjhxzb.cn>

References:

- [1] Su H, Lin Y L, Wang Z H, Wong Y L E, Chen X F, Chan T W D. Magnetic Metal-Organic Framework-Titanium Dioxide Nanocomposite as Adsorbent in the Magnetic Solid-Phase Extraction of Fungicides from Environmental Water Samples. *J. Chromatogr. A*, **2016**,**1466**:21-28
- [2] Kurt-Karakus P B, Ugranli-Cicek T, Sofuoglu S C, Celik H, Gungormus E, Gedik K, Sofuoglu A, Okten H E, Birgul A, Alegria H, Jones K C. The First Countrywide Monitoring of Selected POPs: Polychlorinated Biphenyls (PCBs), Polybrominated Diphenyl Ethers (PBDEs) and Selected Organochlorine Pesticides (OCPs) in the Atmosphere of Turkey. *Atmos. Environ.*, **2018**,**177**:154-165
- [3] Yan W, Zhang C L, Chen S G, Han L J, Zheng H G. Two Lanthanide Metal-Organic Frameworks as Remarkably Selective and Sensitive Bifunctional Luminescence Sensor for Metal Ions and Small Organic Molecules. *ACS Appl. Mater. Interfaces*, **2017**,**9**(2):1629-1634
- [4] 高玲玲, 牛晓燕, 杜意恩, 胡拖平. 3,5-二(2',5'-苯二羧酸)苯甲酸构筑的金属有机配合物的荧光识别及磁性. *无机化学学报*, **2020**,**36**(7):1383-1392
- GAO L L, NIU X Y, DU Y E, HU T P. Luminescence Sensing and Magnetic Property of Three Metal-Organic Complexes Based on 3,5-Di(2',5'-dicarboxylphenyl)benzoic Acid. *Chinese J. Inorg. Chem.*, **2020**,**36**(7):1383-1392
- [5] Tang J, Ma X H, Yang J, Feng D D, Wang X Q. Recent Advances in Metal-Organic Frameworks for Pesticide Detection and Adsorption. *Dalton Trans.*, **2020**,**49**(41):14361-14372
- [6] Yang Y N, Liu W, Cao J, Wu Y W. On-Site, Rapid and Visual Determination of Hg^{2+} and Cu^{2+} in Red Wine by Ratiometric Fluorescence Sensor of Metal-Organic Frameworks and CdTe QDs. *Food Chem.*, **2020**,**328**:127119
- [7] 翟丽军, 张婕, 高玲玲, 高婷, 贾焦焦, 牛宇岚, 胡拖平. 基于芳香四羧酸构筑的两种配位聚合物的荧光及磁性. *无机化学学报*, **2020**,**36**(1):173-182
- ZHAI L J, ZHANG J, GAO L L, GAO T, JIA J J, NIU Y L, HU T P. Two Coordination Polymers Constructed by Aromatic Tetracarboxylic Acid: Luminescent and Magnetic Properties. *Chinese J. Inorg. Chem.*, **2020**,**36**(1):173-182
- [8] Wang X Q, Feng D D, Tang J, Zhao Y D, Li J, Yang J, Kim C K, Su F. A Water-Stable Zinc(II)-Organic Framework as a Multiresponsive Luminescent Sensor for Toxic Heavy Metal Cations, Oxyanions and Organochlorine Pesticides in Aqueous Solution. *Dalton Trans.*, **2019**,**48**(44):16776-16785
- [9] Xue H, Huang X S, Yin Q, Hu X J, Zhang H Q, Huang G, Liu T F. Bimetallic Cationic Metal-Organic Frameworks for Selective Dye Adsorption and Effective $\text{Cr}_2\text{O}_7^{2-}$ Removal. *Cryst. Growth. Des.*, **2020**,**20**(8):4861-4866
- [10] Sun D, Yan Z H, Blatov V A, Wang L, Sun D F. Syntheses, Topological Structures, and Photoluminescences of Six New Zn(II) Coordination Polymers Based on Mixed Tripodal Imidazole Ligand and Varied Polycarboxylates. *Cryst. Growth Des.*, **2013**,**13**(3):1277-1289
- [11] Zhai Z W, Yang S H, Cao M, Li L K, Du C X, Zang S Q. Rational Design of Three Two-Fold Interpenetrated Metal-Organic Frameworks: Luminescent Zn/Cd-Metal-Organic Frameworks for Detection of 2,4,6-Trinitrophenol and Nitrofurazone in the Aqueous Phase. *Cryst. Growth. Des.*, **2018**,**18**:7173-7482
- [12] Zhang X, Zhuang X R, Zhang N X, Ge C Y, Luo X, Li J X, Wu J, Yang Q F, Liu R. A Luminescent Sensor Based on a Zn(II) Coordination Polymer for Selective and Sensitive Detection of NACs and Fe^{3+} Ions. *CrystEngComm*, **2019**,**21**(12):1948-1955
- [13] Yan Y T, Zhang W Y, Zhang F, Cao F, Yang R F, Wang Y Y, Hou L. Four New Metal-Organic Frameworks Based on Diverse Secondary Building Units: Sensing and Magnetic Properties. *Dalton Trans.*, **2018**,**47**(5):1682-1692
- [14] Kang X M, Fan X Y, Hao P Y, Wang W M, Zhao B. A Stable Zinc-Organic Framework with Luminescence Detection of Acetylacetone in Aqueous Solution. *Inorg. Chem. Front.*, **2019**,**6**:271-277
- [15] Parsons R, Drickamer H. Effect of Pressure on the Spectra of Certain Transition Metal Complexes. *J. Chem. Phys.*, **1958**,**29**(4):930-937
- [16] Alexander J J, Gray H B. Electronic Structures of Hexacyanometalate Complexes. *J. Am. Chem. Soc.*, **1968**,**90**(16):4260-4271
- [17] Naiman C. Interpretation of the Absorption Spectra of $\text{K}_3\text{Fe}(\text{CN})_6$. *J. Chem. Phys.*, **1961**,**35**:323-328
- [18] Gale R, McCaffery A J. Bonding Studies from Charge-Transfer Absorption and Magnetic Circular Dichroism Spectra. Part II. The Complex Hexacyanoferrate(III) and Pentacyanoferrate(III) Complexes of C_{4v} Symmetry. *Dalton Trans.*, **1973**:1344-1351
- [19] Zhang J, Gao L L, Zhai L J, Wang X Q, Fan L M, Hu T P. Gas Adsorption, Magnetic, and Fluorescent Sensing Properties of Four Coordination Polymers Based on 1,3,5-Tris(4-carboxylphenyloxy)benzene and Bis(imidazole) Linkers. *CrystEngComm*, **2018**,**20**(47):7666-7676
- [20] Tao C L, Chen B, Liu X G, Zhou L J, Zhu X L, Cao J, Gu Z G, Zhao Z J, Shen L, Tang B Z. A Highly Luminescent Entangled Metal-Organic Framework Based on Pyridine-Substituted Tetraphenylethene for Efficient Pesticide Detection. *Chem. Commun.*, **2017**,**53**(72):9975-9978
- [21] Qin G X, Wang J, Li L, Yuan F F, Zha Q Q, Bai W B, Ni Y H. Highly Water-Stable Cd-MOF/ Tb^{3+} Ultrathin Fluorescence Nanosheets for Ultrasensitive and Selective Detection of Cefixime. *Talanta*, **2021**,**221**:121421
- [22] Wang X Q, Ma X H, Feng D D, Tang J, Wu D, Yang J, Jiao J J. Four Novel Lanthanide(III) Metal-Organic Frameworks: Tunable Light Emission and Multiresponsive Luminescence Sensors for Vitamin B-6 and Pesticides. *Cryst. Growth Des.*, **2021**,**2**(5):2889-2897